ELECTRO-MECHANICAL IMPACT SYSTEM EXCITED BY A SOURCE OF LIMITED POWER

Ladislav Půst*

Electromechanical system with one degree of freedom in mechanical oscillating part and with other degrees in rotation a electrical subsystems is investigated by means of numerical solution of derived equations in dimensionless form. The most important nonlinearities are impacts of the main body on the stiff but deformable stop. Other nonlinear effects are introduced into system by the force transformation from unbalance exciter with limited power into the oscillating subsystem and also by nonlinear magnetic flux in the driving electromotor. Presented numerical simulation was focused on the study of the influence of exciting unbalance level on the time histories of oscillations and on phase trajectories. The various responses were shown and discussed in examples.

Key words : *mechanical oscillations, impacts, multiplicative impact damping model, limited power of exciter, electro-mechanical interaction*

1. Introduction

The nonlinear properties of dynamic system have been studied very intensively during the last 50 years, but nonlinearity was mainly considered as consequence of internal nonlinear elements – springs or damping – in the investigated mechanical system. The nonlinearity caused by the non-ideal characteristics of the exciting force source has been taken into account only exceptionally [1–4, 7, 8], in spite of the fact that the energy sources of the real structures are always non-ideal with limited power and limited inertia.

The interaction of such non-ideal source of energy with the nonlinear mechanical system at forced or self-excited vibration can produce new phenomena [10–12], especially at strongly nonlinearities as are impacts, dry friction, clearances, etc. [9].

The presented article is focused on such a case. The impacts are supposed to be soft but sufficiently strong and with different losses of kinetic energy during contact. Mechanical system has one degree of freedom and the source of excitation is an unbalance exciter driven by an electromotor with nonlinearity in the inner electromagnetic circuit.

2. Electro-mechanical system

Such a system in its simplest form is shown in Fig. 1. It consists of a mechanical subsystem build of mass m, linear springs s with stiffness k, linear dashpot with damping coefficient b and an nonlinear stop with characteristic $f(x, \dot{x}_1)$, (where $x_1 = x - r$) and with clearance r in the equilibrium position. This subsystem is excited by the centrifugal exciter with unbalance $m_n e$, driven by electrical motor with moment of inertia I_m. Mass of this mo-

* Ing. L. Půst, DrSc., Institute of Thermomechanics AS CR, v.v.i., Dolejškova 5, 18200 Praha 8

tor is included into the mass m, which can move only in the vertical direction, due to the parallel leaf springs S.

Rotor of the electric motor rotates with a angular velocity $\dot{\varphi} = \mathrm{d}\varphi/\mathrm{d}t$ and is driven by the electromagnetic moment $M_{\mathrm{em}} = r\, c\, \Phi(i)\, i$ dependent on the current i, where r is radius of motor gap, $c\,\Phi(i)$ is magnetic flux roughly constant at the permanent magnet, but increasing with current i at electromagnet. Current i is generated in the electric circuits with elements L, R, $c\,\Phi(i)$ of motor fed by the prescribed voltage U, which we suppose to be constant or slowly varying in time.

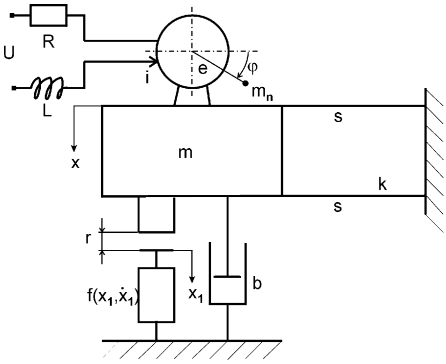

Fig.1: Electromechanical system

3. Mathematical model of 1DOF mechanical subsystem

The forced vibration of 1DOF mechanical subsystem is described by equation

$$m\,\ddot{x} + b\,\dot{x} + k\,x + f(x,\dot{x}) = m_{\mathrm{n}}\, e\,(\dot{\varphi}^2 \sin\varphi - \ddot{\varphi}\cos\varphi)\ , \tag{1}$$

where the function $f(x,\dot{x})$ describes the impact stop characteristic, which we suppose to be viscous-elastic. The corresponding hysteretic loop is shown in Fig. 2a and its mathematical description is:

$$f(x,\dot{x}) = k_{\mathrm{c}}\,(x-r)\,(1 - b_{\mathrm{c}}\,\dot{x})\,H(x-r)\ , \tag{2}$$

where k_{c} [$\mathrm{kg\,s^{-2}}$] and b_{c} [$\mathrm{s\,m^{-1}}$] are stiffness coefficient and damping parameter of stop, $H(x-r)$ is Heaviside function, $H = 0$ for $x \le r$, $H = 1$ for $x > r$.

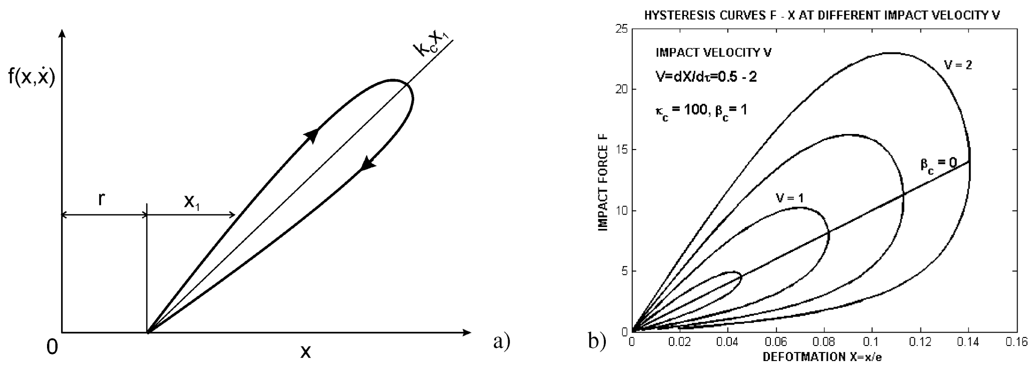

Fig.2: a) impact hysteresis loop; b) hysteresis loops at different impact velocities

We use here the so called 'multiplicative model' of the impact damping, where the deformation function $k_{\mathrm{c}}\,(x-r)$ is multiplied by a function of velocity $(b_{\mathrm{c}}\,\dot{x})$. The advantages of this model in comparison to the classical 'additive model' $(k_{\mathrm{c}}\,(x-r) + b_{\mathrm{c}}\,\dot{x})$ are proved in [15, 16]. The properties of different impact velocities on the hysteresis loop are shown in Fig. 2b.

The energy input into the oscillating system is given by the rotation of rotor with instantaneous angular velocity $\dot{\varphi}$ [5, 6] determined by the equation

$$I_{\mathrm{m}}\,\ddot{\varphi} = -M_{\mathrm{z}} + r\,c\,\Phi(i)\,i - e\,m_{\mathrm{n}}\,\ddot{x}\cos\varphi\ , \tag{3}$$

where M_z is resistance moment. The last expression on the right hand side of eq. (3) gives the feedback loop force of oscillating system motion $x(t)$ on the centrifugal exciter.

Current i, contained in the active driving electromagnetic moment $r\,c\,\Phi(i)\,i$ is generated in the electric circuit controlled by the voltage U and described for the direct current electric motor by the following differential equation

$$L(i)\,\frac{\mathrm{d}i}{\mathrm{d}t} + R\,i + r\,c\,\Phi(i)\,\dot{\varphi} = U(t)\ . \tag{4}$$

The resistance R is supposed to be constant for the used range of current i. The inductivity $L(i)$ and magnetic flux $\Phi(i)$ change their values with current i in larger scale then the resistance R. In this contribution the nonlinear function of magnetic flux is considered. The magnetic saturation of iron causes the weak nonlinearity of magnetic flux characteristic, which can be expressed by the 'arctg' function [13]

$$\Phi = \Phi_\mathrm{m}\,\frac{2}{\pi}\ \mathrm{arctg}\left(\frac{\pi}{2}\,\frac{i}{i_\mathrm{k}}\right) \tag{5}$$

drawn in Fig. 3. This curve has the tangent in origin

$$\left(\frac{\mathrm{d}\Phi}{\mathrm{d}i}\right)_{i=0} = \frac{\Phi_\mathrm{m}}{i_\mathrm{k}}\ , \tag{5a}$$

where Φ_m $[\mathrm{kg\,m\,s^{-2}\,A^{-1}}]$ is the maximum asymptotic magnetic field for $i \to \infty$.

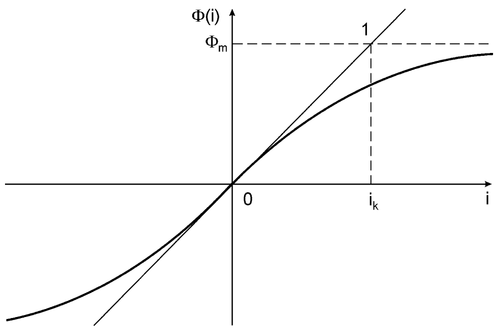

Fig.3: Proposed magnetic saturation curve

Point 1 of intersection of asymptotic flux Φ_m with tangent in origin gives the characteristic current i_k.

Equations $(1, 3, 4)$ contain 18 dimension parameters or variables.

Simpler form of these equations can be get by introducing the dimensionless variables, with using e, k, r and Φ_m as the comparison values:

$$\begin{gathered}
X = \frac{x}{e}\ , \qquad \tau = t\,\sqrt{\frac{k}{m}}\ , \qquad \beta = \frac{b}{\sqrt{k\,m}}\ , \qquad \tilde{f}(X, X') = \frac{f(x, \dot{x})}{k\,e}\ , \qquad \Theta = \frac{I_\mathrm{m}}{m\,e^2}\ , \\
\mu_\mathrm{z} = \frac{M_\mathrm{z}}{k\,e^2}\ , \qquad RR = \frac{R\,i_\mathrm{k}}{r\,\Phi_\mathrm{m}}\,\sqrt{\frac{m}{k}}\ , \qquad I = \frac{i}{i_\mathrm{k}}\ , \qquad \Lambda = \frac{L\,i_\mathrm{k}}{r\,\Phi_\mathrm{m}}\ , \\
u = \frac{U}{r\,\Phi_\mathrm{m}}\,\sqrt{\frac{m}{k}}\ , \qquad \mu_\mathrm{n} = \frac{m_\mathrm{n}}{m}\ , \qquad \varrho = \frac{r}{e}\ , \qquad \delta = \frac{i_\mathrm{k}\,\Phi_\mathrm{m}}{e\,k}\ , \qquad \tilde{\Phi} = \frac{\Phi(i)}{\Phi_\mathrm{m}}\ .
\end{gathered} \tag{6}$$

The equations of motion in the dimensionless form using these only 14 dimensionless parameters are

$$\begin{gathered}
\Lambda\,I' + RR\,I + c\,\tilde{\Phi}\,\varphi' = u\ , \\
\Theta\,\varphi'' = -\mu_\mathrm{z} + \varrho\,I\,c\,\tilde{\Phi}\,\delta - \mu_\mathrm{n}\,X''\,\cos\varphi\ , \\
X'' + \beta\,X' + X + \tilde{f}(X, X') = \mu_\mathrm{n}\,[\varphi'^2\,\sin\varphi - \varphi''\,\cos\varphi]\ ,
\end{gathered} \tag{7}$$

where we use the symbol $(\,)' = \mathrm{d}(\,)/\mathrm{d}\tau$.

Variable φ and parameter c, which depends on the internal design of electromotor, are dimensionless and therefore they do not change during the transformation. Two expressions of (2) and (5) of nonlinear functions have to be considered in addition to equations (7) and transformed.

Using dimensionless magnitudes

$$rr = \frac{r}{e}\ , \qquad \kappa_{\mathrm{c}} = \frac{k_{\mathrm{c}}}{k}\ , \qquad \beta_{\mathrm{c}} = b_{\mathrm{c}}\, e \sqrt{\frac{k}{m}}$$

it gives

$$\tilde{f}(X, X') = \kappa_{\mathrm{c}}\, (X - rr)\, (1 + \beta_{\mathrm{c}}\, X')\, H(X - rr)\ . \tag{2a}$$

Similarly we obtain

$$\tilde{\Phi} = \frac{2}{\pi}\ \mathrm{arctg}\left(\frac{\pi}{2}\, I\right)\ . \tag{5b}$$

For easy numerical solution it is useful to eliminate the derivatives X'' from the second equation (7) and derivatives φ'' from the third equation. We get

$$\begin{gathered} \Lambda\, I' + RR\, I + c\, \frac{2}{\pi}\ \mathrm{arctg}\left(\frac{\pi}{2}\, I\right) \varphi' = u\ , \\ (\Theta + \mu_{\mathrm{n}}^2\, \cos^2\varphi)\, \varphi'' = -\mu_{\mathrm{z}} + \varrho\, I\, c\, \frac{2}{\pi}\ \mathrm{arctg}\left(\frac{\pi}{2}\, I\right) \delta - \\ - \mu_{\mathrm{n}}\, \cos\varphi\, [-\beta\, X' - X - \tilde{f}(X, X') + \mu_{\mathrm{n}}\, \varphi'^2 \sin\varphi]\ , \\ \left(1 - \frac{\mu_{\mathrm{n}}^2 \cos^2\varphi}{\Theta}\right) X'' + \beta\, X' + X + \tilde{f}(X, X') = \mu_{\mathrm{n}} \left[\varphi'^2 \sin\varphi - \frac{(-\mu_{\mathrm{z}} + \varrho\, I\, c\, \tilde{\Phi}\, \delta)\, \cos\varphi}{\Theta}\right]\ . \end{gathered} \tag{8}$$

If a small voltage U feeds the excitation of this electromechanical system, then the magnetic characteristic can be simplified to $\tilde{\Phi} = I$.

Analogous, if motion in mechanical subsystem would be realized without any impacts, $\tilde{f}(X, X') = 0$, then equations (8) are simple:

$$\begin{gathered} \Lambda\, I' + RR\, I + c\, I\, \varphi' = u\ , \\ (\Theta + \mu_{\mathrm{n}}^2\, \cos^2\varphi)\, \varphi'' = -\mu_{\mathrm{z}} + \varrho\, c\, I^2\, \delta - \mu_{\mathrm{n}}\, \cos\varphi\, [-\beta\, X' - X + \mu_{\mathrm{n}}\, \varphi'^2 \sin\varphi]\ , \\ \left(1 - \frac{\mu_{\mathrm{n}}^2 \cos^2\varphi}{\Theta}\right) X'' + \beta\, X' + X = \mu_{\mathrm{n}} \left[\varphi'^2 \sin\varphi - \frac{(-\mu_{\mathrm{z}} + \varrho\, c\, I^2\, \delta)\, \cos\varphi}{\Theta}\right]\ . \end{gathered} \tag{9}$$

The equations (8) are used for numerical solutions of the motion of studied electromechanical system.

4. Examples

A) The equations of motion contain a lot of parameters describing investigated system. We will focus on the influence of increasing amplitude of excitation, defined by dimensionless parameter $\mu_{\mathrm{n}} = m_{\mathrm{n}}/m$, on the type of oscillations.

Other parameters are supposed to be constant: damping of mechanical system $\beta = 0.04$, moment of inertia $\Theta = 30$, loading moment $\mu_{\mathrm{z}} = 0.01$, stiffness of stop $k_{\mathrm{c}} = 100$ and its damping $\beta_c = 0.1$, clearance between stop and main mass m at its central position $rr = 0.5$, resistance $RR = 1$, ratio of electric and mechanic values $\delta = 0.2$ and feeding voltage $u = 2$.

Response on the small excitation given by the mass ratio $\mu_n = m_n/m = 0.1$ is very near to harmonic motion shown in Fig. 4. The mass m touches the stop very slightly at its maximum displacement, which is seen from the short vertical straight line in the phase plane trajectory in Fig. 5. The mechanical motion is periodic with constant revolutions containing very small disturbances.

This motion can be however strongly influenced by the transient oscillations at general initial conditions. Therefore we begin the solution always firstly with roughly estimated initial conditions X, X', η, I, φ and consider record for a long dimensionless time τ (e.g. $\tau_{max} = 200$), sufficient for reverberation of these disturbing components. The gained end conditions X, X', η, I, φ were then (after repetition if necessary) used as initial conditions for records presented in the article. Small distortions, as well as their reverberations, are seen on the left sides of records in Fig. 4, 6, 8, 10. The right sides of these time histories records (e.g. $\tau = 60$–120) were then applied for creation of phase plane trajectories (Fig. 5, 7, 9, etc.).

Twice greater excitation $\mu_n = 0.2$ changes considerably the type of oscillations. Time histories of displacement X (upper record) and of dimensionless velocity V (bottom record)

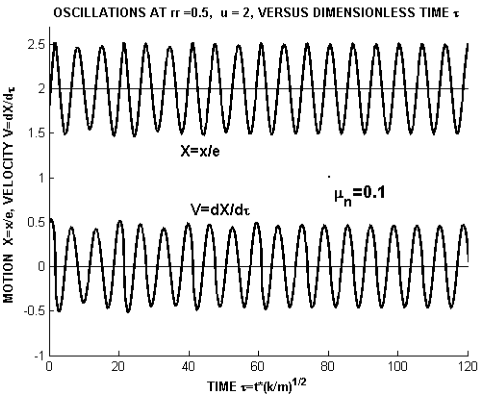

Fig.4: Time history of displacement and velocity at slight impact

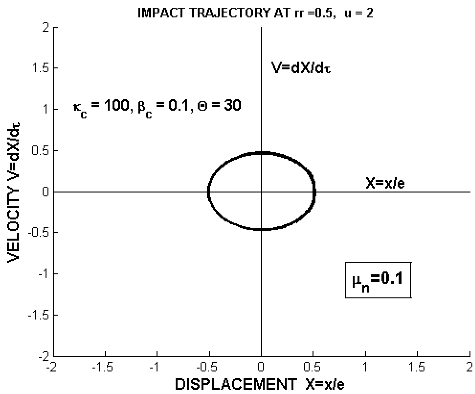

Fig.5: Phase trajectory at slight impact, unbalance $\mu_n = 0.1$

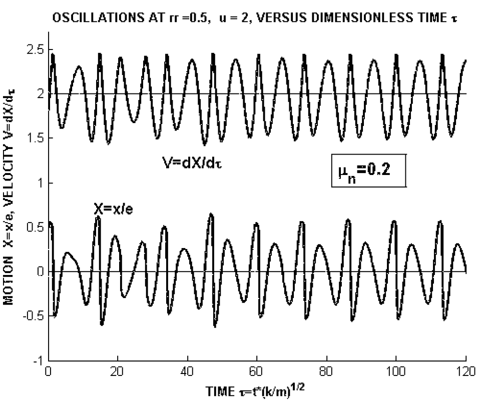

Fig.6: Time history of displacement and velocity, unbalance $\mu_n = 0.2$

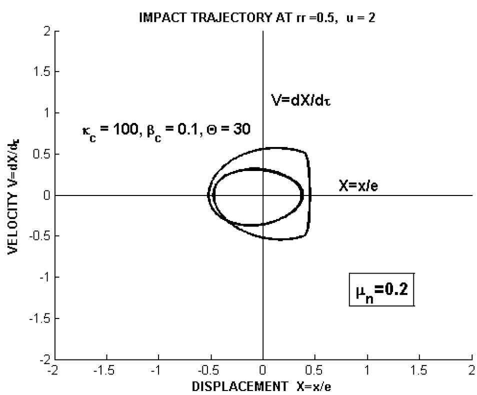

Fig.7: Phase trajectory at unbalance $\mu_n = 0.2$

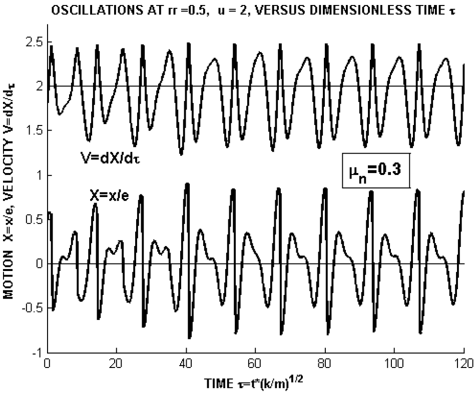

Fig.8: Time history of displacement and velocity, unbalance $\mu_{\mathrm{n}} = 0.3$

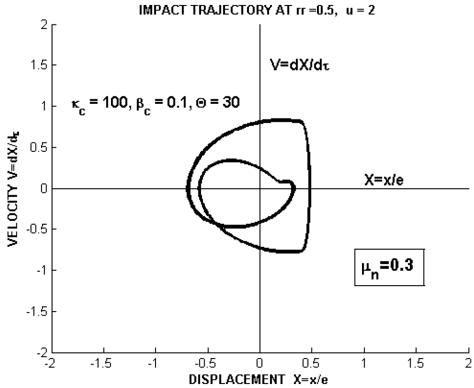

Fig.9: Phase trajectory at unbalance $\mu_{\mathrm{n}} = 0.3$

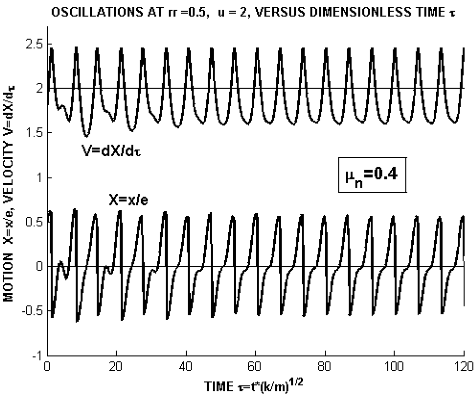

Fig.10: Time history of displacement and velocity, unbalance $\mu_{\mathrm{n}} = 0.4$

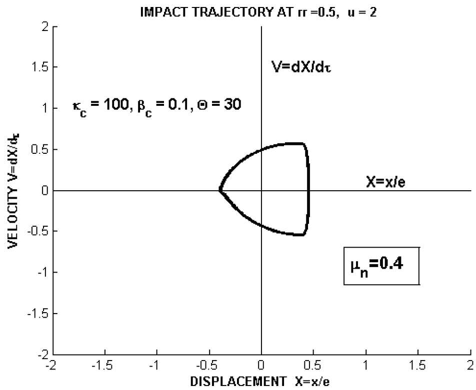

Fig.11: Phase trajectory at unbalance $\mu_{\mathrm{n}} = 0.4$

show the impacts in every second period (Fig. 6) – peaks in X, τ and vertical jump in V, τ record. This jump is distinct in Fig. 7. Due to the small damping in impact $\beta_{\mathrm{c}} = 0.1$ and nonlinear characteristic shown in Fig. 2, the incidence and reversal velocities are roughly the same but with opposite sign.

The similar oscillations with double period is gained at excitation with three times heavier unbalance $\mu_{\mathrm{n}} = 0.3$ and shown in Fig. 8. Nonlinear impact effects – sharp peaks in X, τ and jumps in V, τ – are emphasized, double period keeps.

The similar is also the phase plane portrait shown in Fig. 9, with an additional bump in the inner loop. This bump is evident also in the course of velocity in the previous Figure.

Further increase of excitation to $\mu_{\mathrm{n}} = 0.4$ (Fig. 10) surprisingly change the intensity of oscillations to the lower level and the motion returns to the one-period oscillations, very similar to the oscillations at $\mu_{\mathrm{n}} = 0.1$ (Fig. 4) but with strong impacts.

Interesting form has also the trajectory of motion in phase plane X, V, shown in Fig. 11. The triangular form consists of the quick jump of velocity V from $V \cong 0.6$ to $V \cong -0.6$ at $X \cong 0.5$. The two other sides intersect in the point $X \cong -0.4$, where the velocity stays near zero for a long time (approximately 1/4 period – see Fig. 10). The absolute displacement of this point from origin is smaller than the displacement on the side of the stop.

Another view on the vibration of the impact we can get, if we draw the displacement and velocity versus dimensionless frequency $\eta = \omega\,\sqrt{m/k}$. This is done in Fig. 12, where at slowly decreasing frequency is the displacement drawn in the upper half of Figure, in the middle is the time τ reduced 100 times and in bottom is the course of velocity. The fluctuation of angular velocity η during the monotone increasing time τ and also the deformation of displacement X and velocity V is clearly evident.

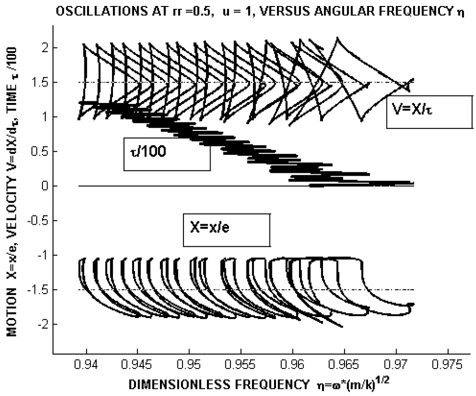

Fig.12: Displacement X and velocity V versus angular frequency η

B) In comparison with the previous example, the mass of unbalance is constant: $\mu_\mathrm{n} = m_\mathrm{n}/m = 0.2$, but the clearance $rr = r/e$ is variable. The further physical quantities are also constant: $\beta = b/\sqrt{km} = 0.05$, $\Theta = I_m/(m\,e^2) = 30$, $\mu_\mathrm{z} = M_\mathrm{z}/(k\,e^2) = 0.15$, $\Lambda = L\,i_\mathrm{k}/(r\,\Phi_\mathrm{m}) = 1$, $\varrho = r/e = 1$, $\delta = i_\mathrm{k}\,\Phi_\mathrm{m}/(e\,k) = 0.2$, $RR = R\,i_\mathrm{k}\,\sqrt{m/k}/(r\,\Phi_\mathrm{m}) = 1$. The parameters of the stop are $\kappa_\mathrm{c} = k_\mathrm{c}/k = 100$ and ten times higher impact damping than is: $\beta_\mathrm{c} = b_\mathrm{c}/\sqrt{km} = 1$. The input voltage has to be increased to $u = U\,\sqrt{m/k}/(r\,\Phi_\mathrm{m}) = 2.8$ in order to hold the system in resonance. The clearance rr is selected from a maximum one $rr > 3$ to a stepwise decreasing $rr = 2, 1, 0$.

Phase trajectories are recorded in Figures 13–16. The impact-less system ($rr > 3$) oscillate very near harmonic motion with amplitude $X = x/e = 2.68$ represented by an ellipse shown in Fig. 13. Drawing the stop nearer to the mass m on the distance $rr = 2$ reduces the maximum displacement in negative direction $X = -2.2$ and to $X = 2.08$ in positive displacement. In Fig. 14 is also seen that the incidence velocity $V_\mathrm{i} = \mathrm{d}X/\mathrm{d}\tau = 1.05$ and returning (reflecting) velocity $V_\mathrm{r} = -0.7$.

Further decreasing of the clearance on the value $rr = 1$ (Fig. 15) reduces again the vibration of mechanical subsystem. The maximum displacements are $X = -1.42$ and 1.09 and the incidence and reflecting velocities are $V_\mathrm{i} = 1.35$ and $V_\mathrm{r} = -0.6$.

The total removal of clearance on $rr = 0$ causes the strong minimization and deformation of phase trajectory X, V as shown in Fig. 16. The incidence and reflecting impact velocities are $V_\mathrm{i} = 1.2$ and $V_\mathrm{r} = -0.618$.

If we illustrate the motion of mechanical subsystem in time histories $X(\tau)$ and $V(\tau)$, we get for the high clearances $rr > 3$ and $rr = 2$ roughly harmonic courses of vibrations. Greater differences from harmonic forms occur at the smaller clearances. Time histories dimensionless displacement X (full line) and velocity V (dashed line) for $rr = 1$ are drawn in Fig. 17. Maximums X are sharp, given by the jump off from the stop. In the same times τ

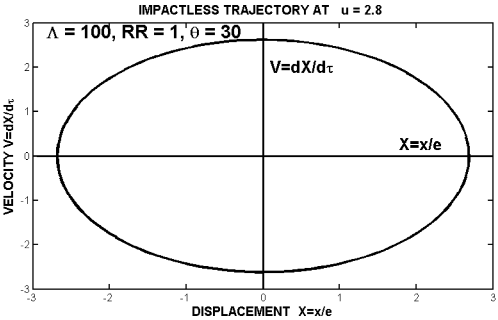

Fig.13: Phase trajectory at impactless motion

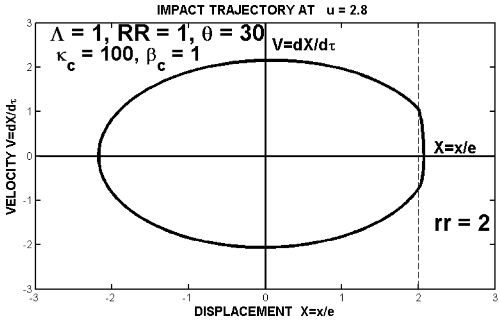

Fig.14: Phase trajectory, impacts at $rr = 2$

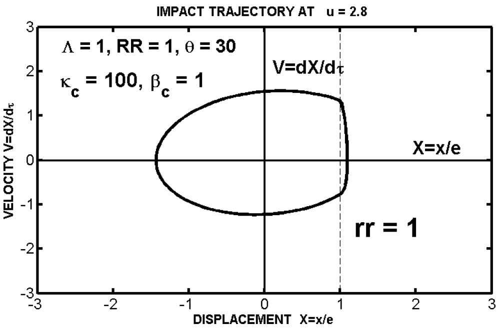

Fig.15: Phase trajectory, impacts at $rr = 1$

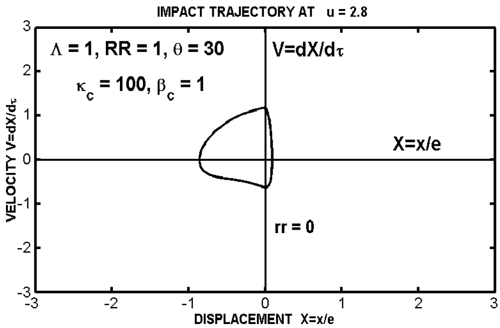

Fig.16: Phase trajectory, impacts at $rr = 0$

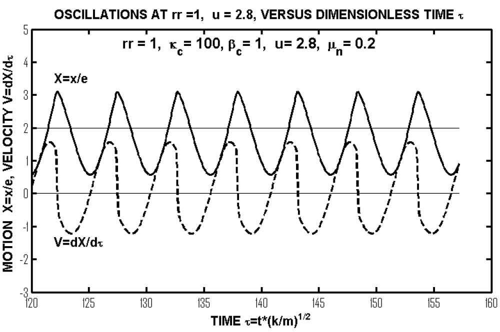

Fig.17: Time histories X and V, impacts at $rr = 1$

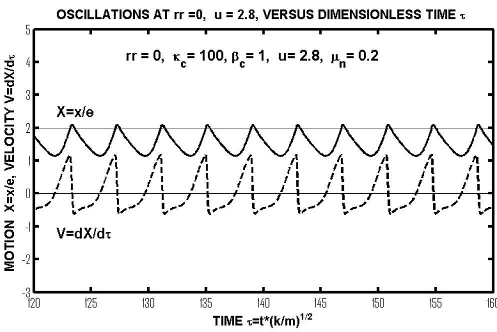

Fig.18: Time histories X and V, impacts at $rr = 0$

of impacts, the velocities V jump from the positive to negative values approximately along the vertical straight lines. These phenomena are even more emphasized in Fig. 18, where the displacement X and velocity V versus time τ are plotted for the system with zero clearance $rr = 0$.

The bottom record $V(\tau)$ in Fig. 18 can be used also for determination of equivalent coefficient of restitution [15] by means of ratio of extreme values (beginning and end of impact) of negative reflecting velocity (V_r) and positive, incidence one (V_i). Equivalent coefficient of restitution is then

$$R_\mathrm{e} = \frac{|V_\mathrm{r}|}{V_\mathrm{i}} = \frac{0.618}{1.2} = 0.515\ .$$

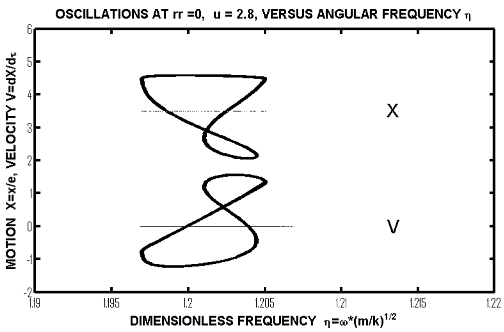

Fig.19: Displacement X and velocity V versus η at $rr = 1$

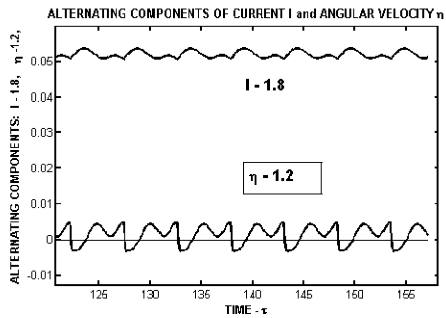

Fig.20: Oscillations of current I and angular frequency η at $rr = 1$

Due to the limited power of the electric motor of the inertia exciter connected with the non-uniform consumption of energy the angular velocity $\dot{\varphi}$ resp. $\eta = \dot{\varphi}\,\sqrt{m/k}$ fluctuates in time. The fluctuations of dimensionless displacements X and velocity V versus angular velocity η are drawn in Fig. 19. Very small displacements X exceeding clearance $rr = 1$ (upper record) correspond to the stop deformation. Roughly horizontal line at maximum value of X graphically represents the sudden drop of angular velocity $\Delta\eta$ during the impact. During this impact, the quick transition of incidence impact velocity $V_{\rm i}$ into negative reflected velocity $V_{\rm r}$ occurs at the simultaneous decrease of angular velocity $\Delta\eta$ what is represented by a oblique straight line in the bottom record $V(\eta)$.

The short stage of alternating component of angular velocity η is in the Fig. 20 bottom. In the interval $\Delta\tau = 40$, there are recorded approx. 7 periods containing not only nearly harmonic change of η caused by the finite power of electric motor, but also the abrupt reduction of angular velocity η during impact, in extent 1 % of average velocity $\eta \approx 1.2$.

Fluctuation of energy consumption by a vibrating system influences also the fluctuation of current $I = i/i_{\rm k}$ in electric circuit of exciter motor, as shown in the record of fluctuating component $(I - 1.8)$ versus time τ in the top of Fig. 20. The impacts become evident here as well, but only by the breaks, not by jump as in $\eta(\tau)$.

All these phenomena can be amplified by further reduction of electric and for mechanic parameters of exciter, e.g. $I_{\rm m}$, r, $\Phi_{\rm m}$, L, R etc. The chaotic motion can occur as well. In the presented examples, the chaos does not appear due to the sufficient damping both in the main electro-mechanical system and in the stop.

5. Conclusion

Mathematical model consisting of three equations describing the behaviour of mechanical oscillating system with impact on a stop with general nonlinear characteristic is derived and transformed into a dimensionless form. This system is driven by an electric motor with limited power and limited inertia. Constant voltage feeds the electric circuits of motor.

The numerical solution of derived dimensionless motion's equation for various values of unbalance mass $\mu_{\rm n} = 0.1$–0.4 shows the different type of oscillations – periodic with one or two periods – as time histories and as phase plane trajectories. The oscillations of mechanical system influence also the angular velocity of driving electromotor and its feeding current.

This article is the extended version of the paper [14].

Acknowledgement

The work was supported by the research project of the Czech Science Foundation No. 101/06/0063 'New computer approaches to investigation of nonlinear and chaotic vibration of rotors and drives due to their interaction with the neighbourhood'.

References

[1] Kononěnko V. O.: Nelinějnyje kolebanija mechaničeskich sistěm, Naukova Dumka, Kijev, 1980
[2] Alifov A., Frolov K.V.: Vzajimodějstvije nělinějnych kolebatelnych sistěm s istočnikami energii, Nauka, Moskva, 1985
[3] Balthazar J.J., et. al.: An Overview on Non-Ideal Vibrations, Meccanica 38, 2003, p. 613–621
[4] Brasil R., M., Balthazar J. M.: Nonlinear Oscillations of a Portal Frame Structure Excited by a Non-ideal Motor, In Control of Oscillations and Chaos, ed. Fradkov A.L., IPME RAS, St. Petersburg, 2000, p. 275–278
[5] Kratochvíl C., Krejsa J.: Modeling of drive systems, Inst. of mechanics of solids, VUT Brno, 2003
[6] Procházka F., Kratochvíl C.: Úvod do matematického modelování pohonových soustav, AN CERM, Brno, 2002
[7] Slavík J., Stejskal V., Zeman V.: Základy dynamiky strojů, Vyd. ČVUT 1997
[8] Kratochvíl C., Procházka F.: Porovnání dynamických vlastností elektromechanických pohonových soustav se stejnosměrnými motory, Computational Mechanics, ZČU Plzeň, Nečtiny, 2004, p. 231–238
[9] Půst L.: Dynamika kladivového drtiče, In. Inženýrská mechanika '96, Svratka, VUT Brno, 1996, p. 197–202
[10] Půst L.: Vibrations of System Excited by a Motor with Limited Power, 21th conference Computational mechanics 2005, Nečtiny, ZČU, 2005, p. 493–500
[11] Půst L.: Effect of limited-power motor on vibrations of system with closely spaced resonances, In. Computational Mechanics, Nečtiny, ZČU, 2006, p. 497–504
[12] Půst L.: Weak excitation of non-linear rotor system with closely spaced resonances, In. 12^{th} IFTOMM World Congress, Besancon (France), June 18–21, 2007, CD-ROM Edition, p. 504/1–504/6
[13] Půst L.: Nonlinear effects on the rotor driven by a motor with limited power, Applied and Computational Mechanics, Nečtiny, 2007, p. 603–612
[14] Půst L.: Impact system excited by a source of limited power, Colloquium Dynamics of machines 2008, Prague, IT ASCR, 5.–6. 2. 2008, p. 145–152
[15] Půst L.: Equivalent coefficient of restitution, Engineering Mechanics, Vol. 5, 1998, No. 5, pp. 303–318
[16] Půst L.: Models of Weak Stops-Application to 2DOF System, in Proc. 10^{th} World Congress on TMM, Vol. 4, Univ. Oulu, Finland, June 20–24, 1999, pp. 1607–1612

Received in editor's office: March 25, 2008
Approved for publishing: July 7, 2008